

HEFAT2011
8th International Conference on Heat Transfer, Fluid Mechanics and Thermodynamics
11 – 13 July 2011
Pointe Aux Piments, Mauritius

GEOMETRIC OPTIMISATION OF FORCED CONVECTION IN A VASCULARISED MATERIAL

Olakoyejo O.T., Bello-Ochende T.* and Meyer J.P.

*Author for correspondence

Department of Mechanical and Aeronautical Engineering,
 University of Pretoria, Pretoria,
 Private Bag X20, Hatfield 0028,
 South Africa.

E-mail: Tunde.Bello-Ochende@up.ac.za

ABSTRACT

This paper presents a three-dimensional geometric optimisation of cooling channels in forced convection of vascularised material with the localised self-cooling property subject to heat flux. Square configuration was studied for family of porosities. The configuration geometry was optimised in such a way that the peak temperature was minimised at every point in the solid body. The optimisation was subject to the constraint of fixed global volume of solid material, but the elemental volume was allowed to morph. The solid material was subject to heat flux on one side and the cooling fluid was forced through the channels in opposite direction of the heated side of the solid body by the specified pressure difference across the transverse channels in the body. The structure had three degrees of freedom as design variables: elemental volume, channel hydraulic diameter and channel-to-channel spacing. A gradient-based optimisation algorithm was used to determine the optimal geometry that gave the lowest thermal resistance. This optimiser adequately handled the numerical objective function obtained from CFD simulations. The numerical results obtained show that as pressure difference increases, the minimised peak temperature decreases. The results also show the behaviour of the applied pressure difference on the optimised geometry. The use of optimiser made the numerical results to be more robust with respect to the optima internal configurations of the flow systems and dimensionless pressure difference.

INTRODUCTION

Material with the property of self-healing and self-cooling is becoming more promising in heat transfer analysis [1-7]. The development of vascularisation of the material indicates flow architectures that conduct and circulate fluids at every point within the solid body. This solid body (slab) may be performing or experiencing mechanical functions such as mechanical loading, sensing and morphing. This self-cooling

ability of the vascularised material to bathe at every point of a solid body gave birth to the name “smart material”.

Constructal theory and design [8, 9] have been adopted as an optimisation technique for the development of a procedure that is sufficiently allocating and optimising a fixed global space constraint using physical law. The method seeks to optimise the flow architecture that predicts the flow and thermal fluid behaviour in the structure that is subject to global volume constraint. In smart material, constructal theory ideally helps in the vascularisation of the smart material structure by morphing the flow architecture configuration to provide easier and greater access of flow through it. The application of this theory started with Bejan and Sciubba [10], who obtained a dimensionless pressure difference number for optimal spacing of board to board of an array of parallel plate to channel length ratio and a maximum heat transfer density, which can be fitted in a fixed volume in an electronic cooling application using the method of intersection of asymptotes. The applications of this theory have been reviewed [11,12] where, under certain global constraints, the best architecture of a flow system can be achieved with the one that gives less global flow resistances, or allows high global flow access. In other words, the shapes of the channels and the elemental structure that are subject to global constraint are allowed to morph. The optimisation of heat exchanger and multiscale devices by constructal theory have also recently been reviewed and summarised by Reis [13] and Fan and Luo [14].

This paper is borne out of the work of Kim *et al.* [7], who studied theoretical and numerical analysis on vascularised materials with heating from one side and coolant forced from the other side for parallel plate and cylindrical channel configurations in an attempt to find the channel configurations that minimised the non-uniform temperature distribution of vascularised solid body. The study focuses on the optimisation of flow and geometry configuration in a laminar forced convection cooling of vascularised solid with square channels. It examines the optimisation of a fixed and finite global volume

of solid materials with array of square cooling channels, which experience a uniform heat flux from one side. The objective is the building of a smaller construct to form a larger construct body with function of self-cooling that will lead to the minimisation of the global thermal resistance or, inversely, the maximisation of the heat transfer rate density (the total heat transfer rate per unit volume). This is achieved by designing the body in a vascularised manner and forcing a coolant to the heated spot in a fast and efficient way so as to drastically reduce the peak temperature at any point inside the volume that needs cooling.

NOMENCLATURE

Be	[-]	Dimensionless pressure drop number
P	[Pa]	Pressure
Re	[-]	Reynolds number
Pr	[-]	Prandtl number
\dot{q}	[W/m ²]	Heat flux
C_p	[J/kgK]	Specific heat at constant pressure
T	[°C]	Temperature
T_{max}	[°C]	Peak temperature
T_{in}	[°C]	Inlet temperature
H	[m]	Structure height
R	[-]	Thermal resistance
V	[m ³]	Structure volume
W	[m]	Structure width
L	[mm]	Axial length
LFOPC	[-]	Leapfrog Optimisation Program for Constrained Problems
v_{el}	[m ³]	Elemental volume
v_c	[m ³]	Channel volume
w	[mm]	Elemental width
h	[mm]	Elemental height
d_h	[mm]	Hydraulic diameter
s	[mm]	Channel-to-channel spacing
N	[-]	Number of channels
x, y, z	[m]	Cartesian coordinates
n	[-]	Normal
Greek symbols		
k	[W/mK]	Thermal conductivity
α	[m ² /s]	Thermal diffusivity
μ	[kg.s/m]	Viscosity
ν	[m ² /s]	Kinematics viscosity
ρ	[kg/m ³]	Density
∞		Far extreme end
ϕ	[-]	Porosity
Δ	[-]	Difference
i	[-]	Mesh iteration index
γ	[-]	Convergence criterion
Subscripts		
0		Initial extreme end
f		Fluid
in		Inlet
max		Maximum
Min		Minimum
opt		Optimum
out		Outlet
S		Solid

COMPUTATIONAL MODEL

The schematic diagram of physical configuration is shown in figure 1. The system consists of a solid body of fixed global volume V , which is heated with uniform heat flux q'' on the right side; the body is cooled by forcing a single-phase cooling fluid (water) from the left side into the parallel cooling channels. The flow is driven along the length of the channel by a fixed pressure difference ΔP , in a transverse and counter-direction to heat flux. An elemental volume shown in figure 2 consisting of a cooling channel and the surrounding solid was used for analysis because of the assumption of the symmetrical heat distribution on the right side of the structure. The heat transfer in the elemental volume is a conjugate problem, which combines heat conduction in the solid and the convection in the working fluid.

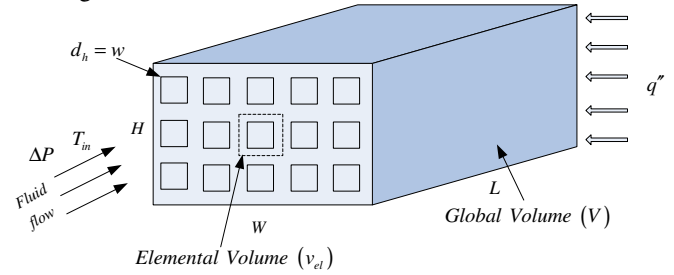


Figure 1. Three-dimensional parallel square channels across a slab with heat flux from one side and forced flow from the other side

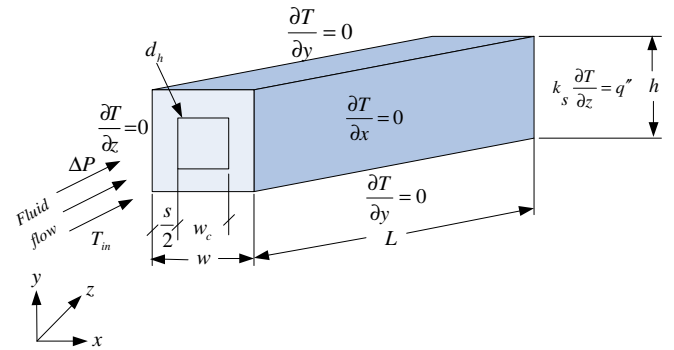


Figure 2. The boundary conditions of the three-dimensional computational domain of the elemental volume

Design variables

In figure 2, an elemental volume v_{el} constraint is considered to be composed of an elemental cooling channel of hydraulic diameter d_h and the surrounding solid of thickness s (spacing between channels) is defined as:

$$w = h \quad (1)$$

$$v_{el} = w^2 L \quad (2)$$

$$w = d_h + s \quad (3)$$

Therefore, the number of channels in the structure arrangement can be defined as:

$$N = \frac{HW}{(d_h + s)^2} \quad (4)$$

However, the void fraction or porosity of the unit structure can be defined as:

$$\phi = \frac{v_c}{v_{cl}} = \left(\frac{d_h}{w}\right)^2 \quad (5)$$

The fundamental problem under consideration is the numerical optimisation of d_h and S , which corresponds to the minimum resistance of a fixed volume for a given pressure drop. The optimisation is evaluated from the analysis of the extreme limits of $(0 \leq d_h \leq \infty)$ and the extreme limits of $(0 \leq s \leq \infty)$.

The optimal values of the design variables within the prescribed interval of the extreme limits exhibit the minimum thermal resistance. The temperature distribution in the model was determined by solving the equation for the conservation of mass, momentum and energy numerically. The discretised three-dimensional computational domain of the configuration is shown in figure. 3. The cooling fluid was water, which was forced through the cooling channels by a specified pressure difference ΔP across the axial length of the structure. The fluid is assumed to be in single phase, steady and Newtonian with constant properties. Water is more promising than air, because air-cooling techniques are not likely to meet the challenge of high heat dissipation in electronic packages [15, 16]. The governing differential equations used for the fluid flow and heat transfer analysis in the unit volume of the structure are:

$$\nabla \cdot \vec{u} = 0 \quad (6)$$

$$\rho(\vec{u} \cdot \nabla \vec{u}) = -\nabla P + \mu \nabla^2 \vec{u} \quad (7)$$

$$\rho_f C_{Pf} (\vec{u} \cdot \nabla T) = k_f \nabla^2 T \quad (8)$$

Energy equation for a solid given as:

$$k_s \nabla^2 T = 0 \quad (9)$$

The continuity of the heat flux at the interface between the solid and the liquid is given as:

$$k_s \frac{\partial T}{\partial n} \Big|_s = k_f \frac{\partial T}{\partial n} \Big|_f \quad (10)$$

A no-slip boundary condition is specified at the wall of the channel,

$$\vec{u} = 0 \quad (11)$$

At the inlet ($x = 0$),

$$u_x = u_y = 0 \quad (12)$$

$$T = T_{in} \quad (13)$$

$$P = \frac{Be\alpha\mu}{L^2} + P_{out} \quad (14)$$

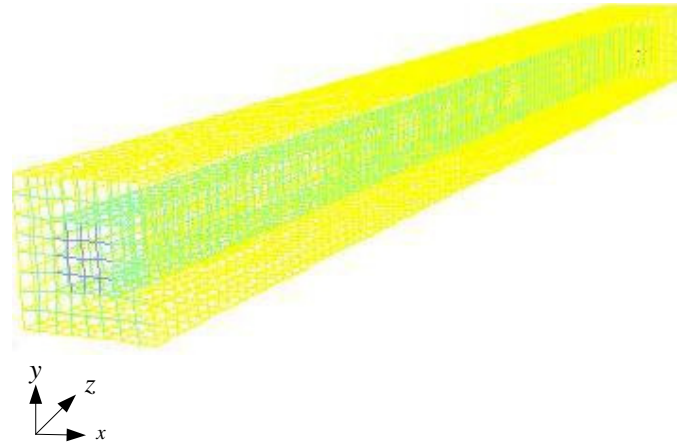


Figure 3. The discretised 3-D computational domain of the elemental solid-fluid volume considered for the simulation

where, Be is the dimensionless pressure difference called Bejan number [17, 18].

At the outlet ($x = L$), zero normal stress

$$P_{out} = 1 \text{ atm} \quad (15)$$

at the left side of the wall, the thermal boundary condition that is imposed is assumed to be:

$$k_s \frac{\partial T}{\partial z} = q'' \quad (16)$$

at the solid boundaries, the remaining outside walls and the plane of symmetry were modelled as adiabatic as shown in figure 2.

$$\nabla T = 0 \quad (17)$$

The measure of performance is the minimum global thermal resistance, which could be expressed in a dimensionless form as:

$$R_{min} = \frac{k_f (T_{max} - T_{in})_{min}}{q''L} \quad (18)$$

And it is a function of the optimised design variables and the peak temperature.

$$R_{min} = f(d_{h_{opt}}, v_{cl_{opt}}, T_{max_{min}}) \quad (19)$$

R_{min} is the minimised thermal resistance for the optimised design variables. The inverse of R_{min} is the optimised overall global thermal conductance.

NUMERICAL PROCEDURE AND GRID ANALYSIS

The simulation work began by fixing the length of the channel, applied pressure difference, porosity, heat flux and material properties and we kept varying values of hydraulic diameter of the channel in order to identify the best (optimal) internal configuration that minimised the peak temperature. The numerical solution of the continuity, momentum and energy Eqs. (6) - (9) along with the boundary conditions (10) - (17) was obtained by using a three-dimensional commercial package

FLUENT™ [19], which employs a finite volume method. The details of the method were explained by Patankar [20]. FLUENT™ was coupled with geometry and mesh generation package GAMBIT [21] using MATLAB [22] to allow the automation and running of the simulation process. After the simulation had converged, an output file was obtained containing all the necessary simulation data and results for the post-processing and analysis. The computational domain was discretised using hexahedral/wedge elements. A second-order upwind scheme was used to discretise the combined convection and diffusion terms in the momentum and energy equations. The SIMPLE algorithm was then employed to solve the coupled pressure-velocity fields of the transport equations. A flow chart representing the numerical procedure is shown in figure 4. The solution is assumed to have converged when the normalised residuals of the mass and momentum equations fall below 10^{-6} and while the residual convergence of energy equation was set to less than 10^{-10} . The number of grid cells used for the simulations varied for different elemental volume and porosities. However, grid independence tests for several mesh refinements were carried out to ensure the accuracy of the numerical results. The convergence criterion for the overall thermal resistance as the quantity monitored is:

$$\gamma = \frac{|(T_{\max})_i - (T_{\max})_{i-1}|}{|(T_{\max})_i|} \leq 0.01 \quad (20)$$

where i is the mesh iteration index. The mesh is more refined as i increases. The $i-1$ mesh is selected as a converged mesh when the criterion (20) is satisfied.

NUMERICAL RESULTS

In this section, we present results for the case when channel hydraulic diameter (or channel width) was in the range of 0.1mm to 1.5mm and the porosities ranged between $0.1 \leq \phi \leq 0.2$ and a fixed length of $L=10\text{mm}$ and fixed applied dimensionless pressure differences of $Be = 10^8$. The thermal conductivity of the solid structure (stainless steel) was 16.27W/m.K ; and the heat flux supplied at left wall was taken to be fixed at 100 kW/m^2 . The thermophysical properties of water [23] used in this study were based on water at 300K and the inlet water temperature was fixed at this temperature.

Figures 5 and 6 show the existence of an optimum hydraulic diameter and elemental volume structure of the cooling channel in which the peak temperature is minimised at any point in the channel for the square configuration studied. Figure 5 shows the graph of peak temperature as a function of the channel hydraulic diameter. It shows that there exists an optimal channel hydraulic diameter, which lies in the range $0.01 \leq d_h/L \leq 0.05$ minimising the peak temperature. Also, the elemental volume of the structure has a strong effect on the peak temperature as shown in figure 6. The minimum peak temperature is achieved when the optimal elemental volume in the range is $0.5\text{mm}^3 \leq v_{el} \leq 8\text{mm}^3$. These indicate that peak temperature decreases as global design variables increase and that optimal values of the design variables are reached beyond

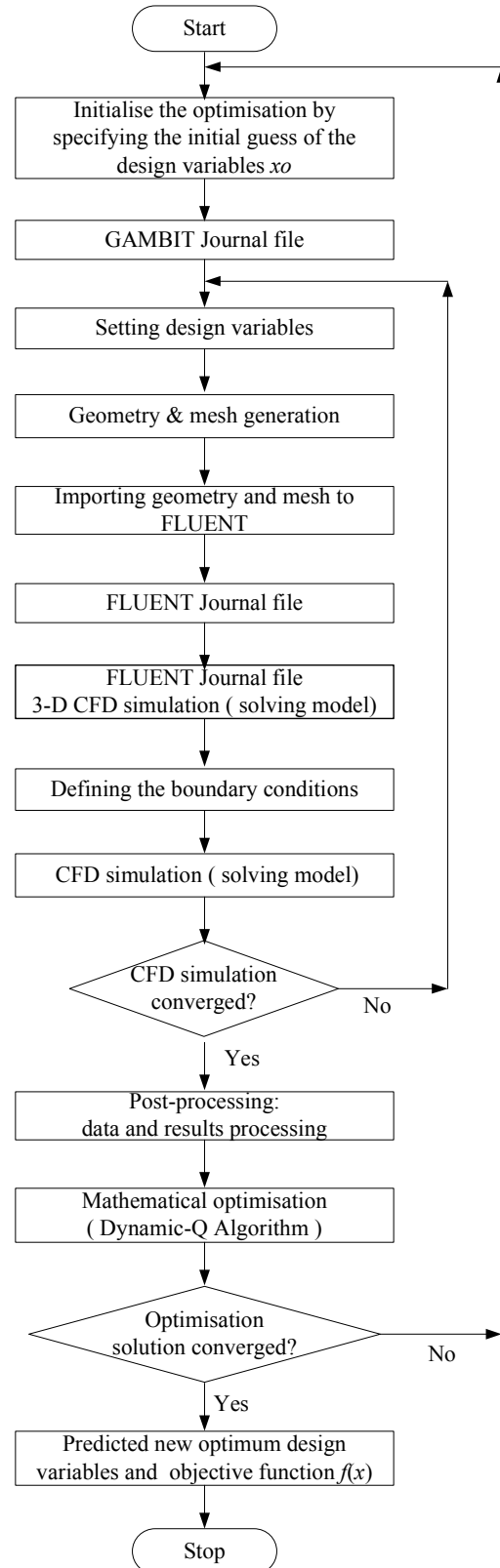


Figure 4. Flow chart of numerical simulation

which the peak temperature begins to increase. Therefore, the global peak temperature decreases as the design variables increase or the global peak temperature decreases as the design variables decrease until it gets to the optimal design values. Any increase or decrease in the design variable beyond the optimal values indicates that the working fluid is not properly engaged in the cooling process, which is detrimental to the global performance of the system. The results show that the optimal arrangement of the elemental volume for the entire structure at this fixed pressure difference should be very small in order to achieve a better cooling. It can also be shown from figures 5 and 6 that porosity has a significant effect on the peak temperature. The best cooling effect occurs at the highest porosity. That is, as the porosity increases, the peak temperature decreases.

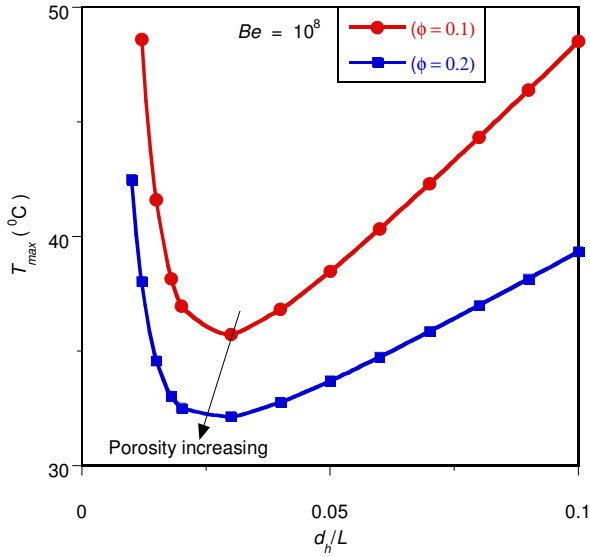


Figure 5. Effect of optimised dimensionless hydraulic diameter d_h on the peak temperature

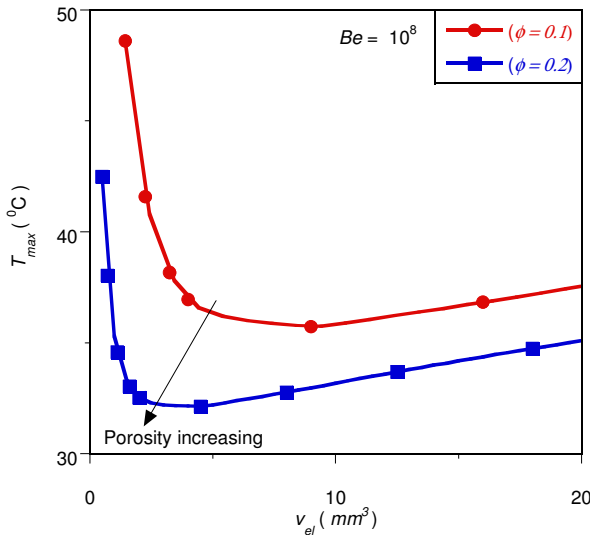


Figure 6. Effect of optimised elemental volume on the peak temperature

MATHEMATICAL OPTIMISATION

In this section, we introduce an optimisation algorithm that will search and identify the optimal design variables at which the system will perform best. A numerical algorithm, Dynamic-Q [24], is employed and incorporated into the finite volume solver and grid (geometry and mesh) generation package by using MATLAB as shown in figure 4 for more efficient and better accuracy in determining the optimal performance.

The Dynamic-Q is a multidimensional and robust gradient-based optimisation algorithm, which does not require an explicit line search. The technique involves the application of a dynamic trajectory LFOPC optimisation algorithm to successive quadratic approximations of the actual problem [25]. The algorithm is also specifically designed to handle constrained problem where the objective and constraint functions are expensive to evaluate. Consider the typical inequality constrained optimisation problem of the following form:

$$\min_x f(x); \left[x_1, \dots, x_2, \dots, x_i, \dots, x_n \right]^T, x_i \in \mathbb{R}^n \quad (21)$$

Subject to

$$g_j(x) \leq 0, j = 1, 2, \dots, p \quad (22)$$

$$h_k(x) = 0, k = 1, 2, \dots, q \quad (23)$$

where, $f(x)$, $g_j(x)$, $h_k(x)$ are scalar functions of the vector x and they are defined as objective function, inequality constraint function and equality constraint function, respectively. The components of vector x are called design variables. An initial guess design $x^{(0)}$ is available, and the solution to the problem is denoted by x^*

The successive approximate quadratic sub-problems, $P[l]$ $l = 0, 1, 2, \dots$ are formed at the successive design point x^l , starting with initial arbitrary design x^0 to a solution x^* by developing the spherical quadratic approximations $\tilde{f}(x)$, $\tilde{g}_i(x)$ and $\tilde{h}_j(x)$ to $f(x)$, $g(x)$ and $h(x)$, respectively. These spherical quadratic approximations are given as:

$$\tilde{f}(x) = f(x^{(l)}) + \nabla^T f(x^{(l)})(x - x^{(l)}) + \frac{1}{2}(x - x^{(l)})^T A(x - x^{(l)}) \quad (24)$$

$$\tilde{g}_i(x) = \tilde{g}_i(x^{(l)}) + \nabla^T \tilde{g}_i(x^{(l)})(x - x^{(l)}) + \frac{1}{2}(x - x^{(l)})^T B_i^{(l)}(x - x^{(l)}), \quad i = 1, \dots, p \quad (25)$$

$$\tilde{h}_j(x) = \tilde{h}_j(x^{(l)}) + \nabla^T \tilde{h}_j(x^{(l)})(x - x^{(l)}) + \frac{1}{2}(x - x^{(l)})^T C_j^{(l)}(x - x^{(l)}), \quad j = 1, \dots, q \quad (26)$$

where $\nabla f(x)$ denotes the gradient vector, A , $B_i^{(l)}$, $C_j^{(l)}$ are approximate Hessian matrices of the objective function, inequality constraint and equality constraint functions, respectively. The approximations are defined by the diagonal matrix as:

$$A = \text{diag}(a, a, \dots, a) = aI, \quad B_i = b_i I, \quad C_j = c_j I \quad (27)$$

The gradient vector of the objective function (obtained from the numerical simulation) at a specified design point x with

respect to each of the design variables x_i is approximated by the first-order forward differencing scheme given as:

$$\frac{\partial f(x)}{\partial x_i} \approx \frac{f(x + \Delta x_i) - f(x_i)}{\Delta x_i} \quad (28)$$

where $\Delta x_i = [0, 0, \dots, \Delta x_i, \dots, 0]^T$ is the suitable step size. The constraint gradient vectors, on the other hand, are provided analytically within the algorithm. The convergence of the solution is in a stable manner and controlled by imposing move limits on the design variables during the optimisation process. The move limit is of the form of single inequality constraints:

$$g_{\delta}(x_i) \left\| x_i - x_i^{l-1} \right\|^2 - \delta_i^2 \leq 0, \quad i = 1, 2, \dots, n \quad (29)$$

where, δ_i is the approximate chosen step limit for each design variable.

The Dynamic-Q algorithm is terminated when either the normalised step size or step function is less than the specified tolerance.

OPTIMISATION PROBLEM

Design variable constraints

The constraint ranges for the optimisation are:

$$0.1 \leq \phi \leq 0.2 \quad (30)$$

$$0.02L \leq w \leq 0.5L \quad (31)$$

$$0 \leq d_h \leq w \quad (32)$$

$$0 \leq s \leq w \quad (33)$$

The design and optimisation technique involves the search for and identification of the best channel layout that minimises the peak temperature, T_{max} such that the minimum thermal resistance between the fixed volume and the cooling fluid is obtained with the desired objectives function. The hydraulic diameter and the channel spacing and elemental volume of the square configuration were considered as design variables. A number of numerical optimisations and calculations were carried out within the design constraint ranges given in (30) – (33) and the results are presented in the succeeding section in order to show the optimal behaviour of the entire system. The elemental volume of the structure was in the range of 0.4mm^3 to 250mm^3 . The optimisation process was repeated for applied dimensionless pressure differences from $Be = 10^6$ to $Be = 10^8$.

Effect of applied pressure difference on optimised geometry and minimised thermal resistance

Figure 7 shows the effect of the minimised thermal resistance as a function of applied dimensionless pressure difference. Minimised thermal resistance decreases as the applied dimensionless pressure difference and porosity increase. Figure 8 shows that the optimal hydraulic diameter decreases as the pressure differences increase and there exists a unique optimal geometry for each of the applied pressure differences. The trend is in agreement with previous work [7].

Effect of material properties on optimised geometry minimised thermal resistance

The effect of material properties on the minimum thermal resistance and optimised internal configuration was also studied. This was best investigated by numerically simulating conjugate heat transfer in an elemental volume for different values of thermal conductivity ratio. Thermal conductivity ratio can be defined as:

$$k_r = \frac{k_s}{k_f} \quad (34)$$

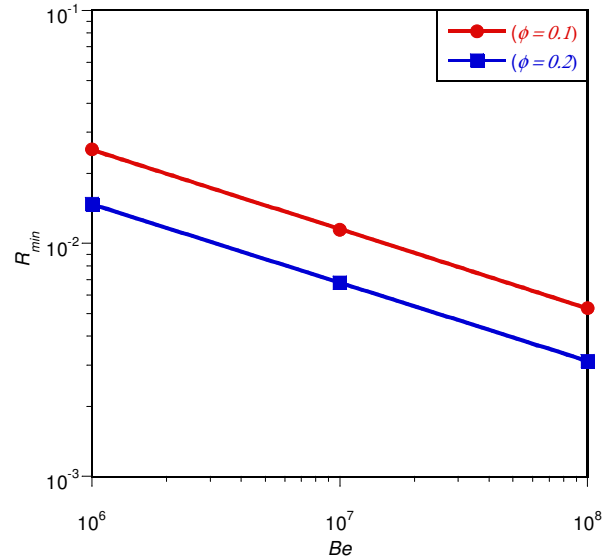


Figure 7. Effect of dimensionless pressure difference on the dimensionless global thermal resistance

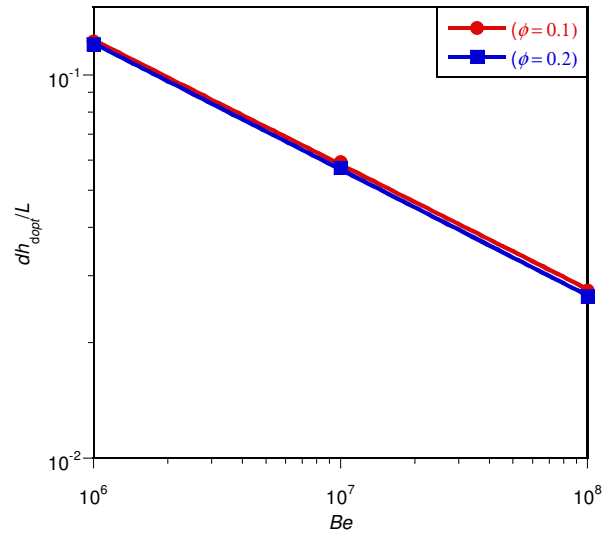


Figure 8. The effect of dimensionless pressure difference on the optimised hydraulic diameter

The numerical simulations follow the same procedure used in section 3 to show the existence of optimal geometry. We started the simulation by fixing $\phi = 0.2$ $Be = 10^8$ and $k_r = 10, 100$.

We then varied the hydraulic diameter and the elemental volume until we got the minimum peak temperature. Figure 9 shows that optimal geometry exists at different effective thermal conductivities and minimum peak temperature is achieved when k_r is high.

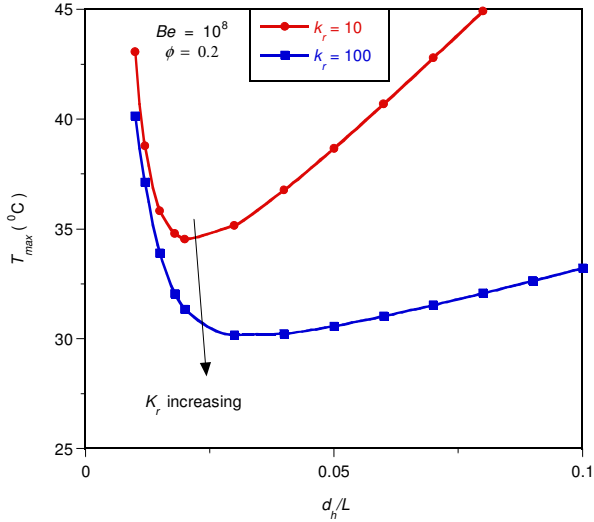


Figure 9. Effect of thermal conductivity ratio k_r on the peak temperature

We later carried on an optimisation process to determine the best geometry that gives us the lowest thermal resistance temperature by using the optimisation algorithm and the procedure in section 5. First of all, we fixed $\phi = 0.2$ and $Be = 10^8$ for all the design constraint ranges and for different values of thermal conductivities ratio ranging from $k_r = 1$ to 10000. Figures 10 and 11 show the effect of the thermal conductivity ratio on the minimised global thermal resistance optimised hydraulic diameter at fixed $\phi = 0.2$ and $Be = 10^8$. The minimised thermal resistance decreases as the thermal conductivity ratio increases. This shows that material properties have strong effect on the thermal resistance. The material with high thermal conductivity property reduces the thermal resistance. Figure 11 shows that thermal conductivity ratio has great influence on optimised hydraulic diameter. As thermal conductivity ratio increases, optimal hydraulic diameter increases. However, at higher thermal conductivity ratio (say $k_r \geq 4000$), the thermal conductivity has negligible effect on minimised thermal resistance and optimised hydraulic diameter.

We later repeated optimisation process for all the design constraint ranges and at $k_r = 1$ to 100 for applied dimensionless pressure differences ranging from $Be = 10^6$ to $Be = 10^8$ and $\phi = 0.1$ to $\phi = 0.2$ to see the global behaviour of the whole system. Figures 12 to 14 show the effect of the applied dimensionless pressure difference on the minimum thermal

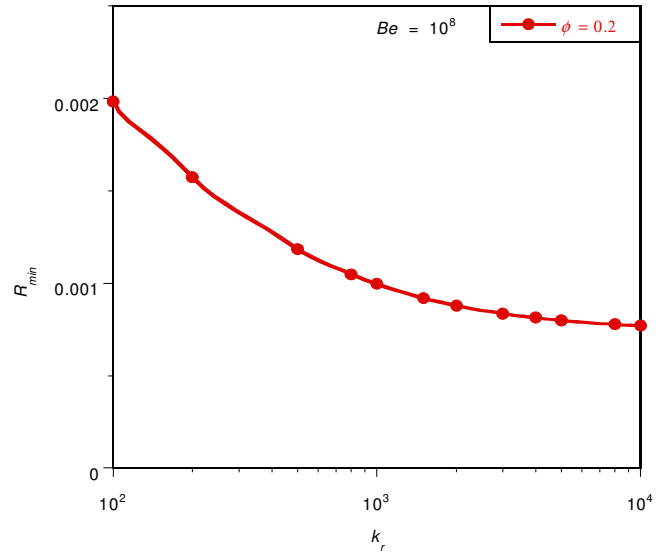


Figure 10. Effect of thermal conductivity ratio k_r on the minimised dimensionless global thermal resistance

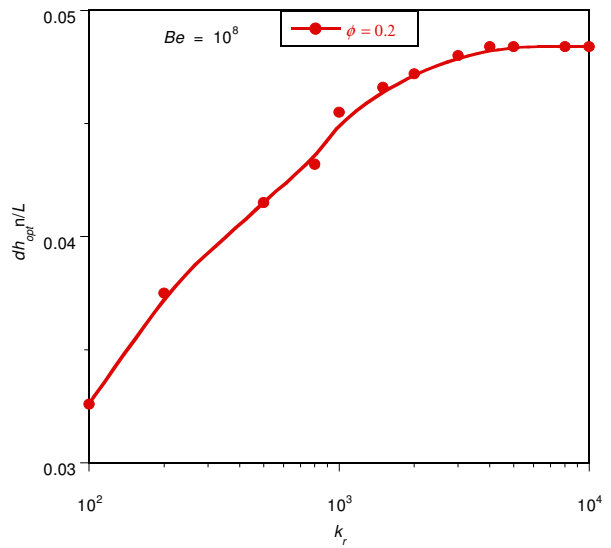


Figure 11. Effect of thermal conductivity ratio k_r on the minimised dimensionless global thermal resistance

resistance and the internal geometry under the influence of thermal conductivity ratio and porosity. Figure 12 shows that the minimised thermal resistance decreases as the applied dimensionless pressure difference, thermal conductivity ratio and porosity increase. Also, figures 13 and 14 show that there is a unique design variable for each applied dimensionless pressure difference, thermal conductivity ratio and porosity.

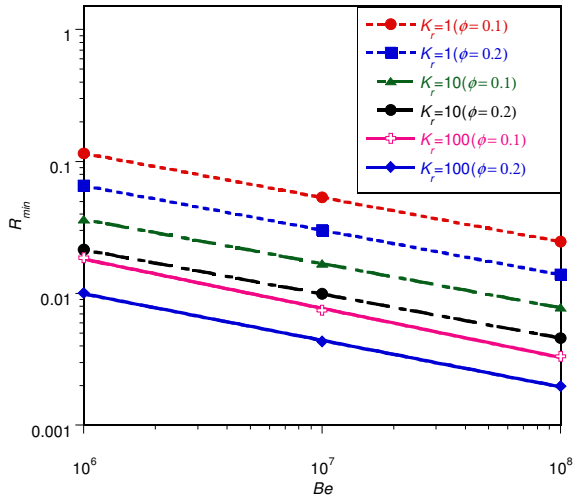


Figure 12. Effect of thermal conductivity ratio k_r and dimensionless pressure difference on the minimised dimensionless global thermal resistance

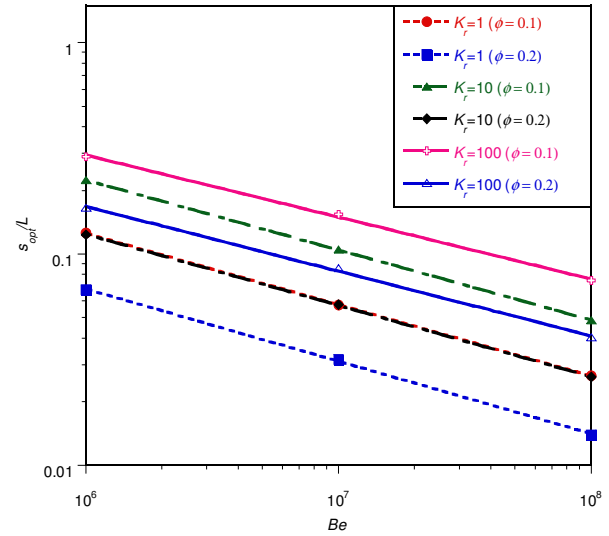


Figure 14. Effect of thermal conductivity ratio k_r and dimensionless pressure difference on the optimised spacing

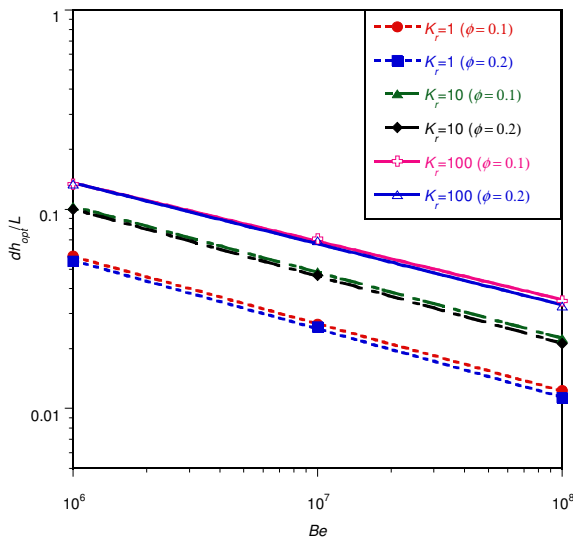


Figure 13. Effect of thermal conductivity ratio k_r and dimensionless pressure difference on the optimised hydraulic diameter

CONCLUSION

This paper studied the numerical optimisation of geometric structures of square cooling channels of vascularised material with the localised self-cooling property subject to heat flux on one side in such a way that the peak temperature is minimised at every point in the solid body. This shows that there are unique optimal design variables (geometries) for a given applied dimensionless pressure number for fixed porosity. The results also show that the material property has great influence on the performance of the cooling channel. Therefore, when designing the cooling structure of vascularised material, the internal and external geometries of the structure,

material properties and pump power requirements are very important parameters to be considered in achieving efficient optimal designs for the best performance.

Future work will investigate the analytical optimisation of this study to confirm this numerical solution

ACKNOWLEDGEMENTS

The authors acknowledge the support of the Department of Mechanical and Aeronautical Engineering, University of Pretoria, and the National Research Foundation for the Republic of South Africa.

REFERENCES

- [1] White S.R., Sottos N.R., Moore J., Geubelle P., Kessler M., Brown E., Suresh S., Viswanathan S., Autonomic healing of polymer composites, *Nature*, vol. 409, 2001, pp. 794–797.
- [2] Reis A.H., Miguel A.F., Bejan A., Constructal theory of particle agglomeration of design of air-cleaning devices, *Journal Physics D: Applied Physics*, vol. 39, 2006, pp. 3086–3096.
- [3] Bejan A., Lorente S., Wang K.-M., Network of channels for self-healing composite materials, *Journal of Applied Physics*, vol. 100, 2006, pp. 033528–033528-6.
- [4] Wang K.-M., Lorente S., Bejan A., Vascularised networks with two optimised channels sizes, *Journal Physics D: Applied Physics*, vol. 39 2006, pp. 3086–3096.
- [5] Kim S.W., Lorente S., Bejan A., Vascularised materials: tree-shaped flow architectures matched canopy to canopy, *Journal of Applied Physics*, vol. 100, 2006, pp. 063525–063525-8.
- [6] Lorente S., Bejan A., Heterogeneous porous media as multiscale structures for maximum flow access,

- Journal of Applied Physics*, vol. 100, 2006, pp. 114909–114909-8.
- [7] Kim S.W., Lorente S., Bejan A., Vascularised materials with heating from one side and coolant forced from the other side, *International Journal of Heat and Mass Transfer*, vol. 50, 2007, pp.3498–3506.
- [8] Bejan A., *Advanced Engineering Thermodynamics*, second ed., Wiley, New York, 1997.
- [9] Bejan A., *Shape and Structure from Engineering to Nature*, Cambridge: Cambridge University Press, UK, 2000.
- [10] Bejan A., Sciubba E., The optimal spacing of parallel plates cooled by forced convection, *International Journal of Heat and Mass Transfer*, vol. 35, 1992, pp. 3259–3264.
- [11] Bejan A., Lorente S., Constructal theory of generation of configuration in nature and engineering, *Journal of Applied. Physics*. vol. 100, 2006, 041301.
- [12] Bejan A., Lorente S., *Design with Constructal Theory*, Wiley, Hoboken, 2008.
- [13] Reis A. H., Constructal theory: from engineering to physics, and how flow systems develop shape and structure, *Applied Mechanics Reviews*, vol. 59, 2006, pp. 269–282.
- [14] Fan Y., Luo, L., Recent applications of advances in microchannel heat exchangers and multi-scale design Optimisation”, *Heat Transfer Engineering*, vol. 29, 2008, pp.461–474.
- [15] Chu R.C., Thermal management roadmap cooling electronic products from handheld device to supercomputers, Proc. MIT Rohsenow Symposium, Cambridge, MA, 2002.
- [16] SEMATECH, The National Technology Roadmap for Semiconductors: Technology, Need SEMATECH, Austin TX, 1997.
- [17] Bhattacharjee S., Grosshandler W.L., The formation of wall jet near a high temperature wall under microgravity environment, *ASME HTD* vol. 96, 1998, pp.711–716.
- [18] Petrescu S., Comments on the optimal spacing of parallel plates cooled by forced convection, *International Journal of Heat and Mass Transfer* vol. 37 1994, pp.1283.
- [19] Fluent Inc., *Fluent Version 6 Manuals*, Centerra Resource Park, 10 Cavendish Court, Lebanon, New Hampshire, USA, 2001 (www.fluent.com).
- [20] Patankar S.V., Numerical heat transfer and fluid flow, hemisphere, New York, 1980.
- [21] Fluent Inc., *Gambit Version 6 Manuals*, Centerra Resource Park, 10 Cavendish Court, Lebanon, New Hampshire, USA, 2001 (www.fluent.com).
- [22] The MathWorks, Inc., *MATLAB & Simulink Release Notes for R2008a*, 3 Apple Hill Drive, Natick, MA, 2008 (www.mathworks.com).
- [23] White F.M., *Viscous Fluid Flow*, 2nd Edition, McGraw-Hill International Editions, Singapore, 1991.
- [24] Snyman J.A., Hay A.M., The DYNAMIC-Q optimisation method: an alternative to SQP?, *Computer and Mathematics with Applications*, vol. 44, 2002, pp. 1589-1598.
- [25] Snyman J.A., *Practical Mathematical Optimisation: An Introduction to Basic Optimisation Theory and Classical and New Gradient-Based Algorithms*, Springer, New York, 2005.